Exponential scaling in early-stage agglomeration of adhesive particles in turbulence

Sheng Chen,[1] Shuiqing Li,[1,*] and Jeffrey S. Marshall[2]
[1]*Key Laboratory for Thermal Science and Power Engineering of Ministry of Education, Department of Energy and Power Engineering, Tsinghua University, Beijing 100084, China*
[2]*Department of Mechanical Engineering, The University of Vermont, Burlington, Vermont 05405, USA*

(Received 22 July 2018; published 26 February 2019)

We carry out direct numerical simulation together with an adhesive discrete element method calculation (DNS-DEM) to investigate agglomeration of particles in homogeneous isotropic turbulence (HIT). We report an exponential-form scaling for the size distribution of early-stage agglomerates, which is valid across a wide range of particle inertia and interparticle adhesion values. Such scaling allows one to quantify the state of agglomeration using a single scale parameter. An agglomeration kernel is then constructed containing the information of agglomerate structures and the sticking probability. An explicit relationship between the sticking probability and microscale particle properties is also proposed based on the scaling analysis of the equation for head-on collisions. Our results extend Smoluchowski's theory to the condition of noncoalescing solid adhesive particles and can reproduce DNS-DEM results with a simple one-dimensional simulation.

DOI: 10.1103/PhysRevFluids.4.024304

I. INTRODUCTION

Clustering of particles suspended in turbulence has been extensively studied in experiments [1,2], in simulations [3], and by theoretical approaches [4,5]. To predict the evolution of cluster or agglomerate size, Smoluchowski's equation, built on statistical collision kernels, is one of the few theoretical tools that can be applied to large-scale systems [6–8]. For particles in turbulence, the collision kernel is usually expressed as the product of the mean relative radial velocity and the radial distribution functions (RDFs) of particle pairs at the distance of contact. For zero-inertia particles, these two quantities can be statistically determined from those of turbulence flows [9]. In contrast, inertial particles preferentially sample certain regions of the flow due to the centrifugation effect, giving rise to higher values of both relative radial velocity and spatial concentration [10–14]. As the inertia of particles further increases, particles from different regions of the flow come together. A larger relative velocity, and consequently a larger collision rate, is then observed. Such effect is termed as "caustics" [15,16] or the "sling effect" [17].

Based on these models of geometric collision kernel, Smoluchowski's theory can be then used to describe the growth of clusters assuming that colliding particles merge immediately to form new larger spherical particles. The assumption of unity coagulation efficiency is normally valid for droplets. However, it is not applicable to the agglomeration of solid *noncoalescing* adhesive particles. Such systems are quite ubiquitous, ranging from electrostatic agglomerators [18], flocculation during water treatment [19], and assemblage of preplanetary grains [20] to the growth of dendrites during aerosol filtration [21,22]. The solid adhesive particles, across 1 to 10^2 microns, have two significant differences from Brownian nanoparticles or coalescing droplets:

*Corresponding author: lishuiqing@tsinghua.edu.cn

(1) The interparticle adhesion due to van der Waals attraction is *short-ranged* and relatively *soft* [23]. It leads to the sticking and rebound behavior of colliding particles (i.e., nonunity coagulation efficiency). (2) Formed agglomerates are usually nonspherical, whose structure will evolve due to restructuring and breakage. It has been reported that even the simplest elastic repulsion between particles considerably changes the picture of agglomeration [24]. Constructing a kernel function that can reflect the influence of complicated interparticle interactions is a crucial problem that has not been settled.

Solving this problem requires a fundamentally different approach—discrete element method (DEM)—that tracks the dynamics of individual particles both while they are traveling alone through the fluid and while they are colliding with other particles [23]. To properly simulate the agglomeration, particle collisions should be resolved with a time step much smaller than the Kolmogorov timescale. Moreover, all the possible modes of particle interaction, i.e., normal impact, sliding, twisting, and rolling, should be taken into account [25,26]. Constructing kernel functions or stochastic agglomeration models [27,28] based on data from DEM simulations then allows large-scale simulation of the agglomeration process.

In this work, we perform direct numerical simulations (DNS) to study the agglomeration of noncoalescing solid particles in homogeneous isotropic turbulence (HIT) with focus on the effect of van der Waals adhesion. An adhesive DEM is employed to fully resolve the translational and rotational motions of particles. We report an exponential-form scaling for the size distribution of early-stage agglomerates as $n(A)/n_0 \sim \exp(-A/\kappa)$, where $n(A)$ is the number density of agglomerates of size A. This exponential distribution allows one to describe the growth of agglomerates using a single scale parameter κ. Based on the simulation results, we are able to extend the Smoluchowski theory to describe adhesion-enhanced agglomeration by introducing a turbulence agglomeration kernel depending on the fractal structure of agglomerates and an adhesion-controlled sticking probability.

II. NUMERICAL METHOD AND SIMULATION CONDITIONS

A. DNS-DEM

1. Fluid phase

In our simulation, the homogeneous isotropic turbulent flow is calculated by DNS on a cubic, triply periodic domain. A pseudospectral method with second-order Adams-Bashforth time stepping is applied to solve the continuity and momentum equations of the incompressible flow,

$$\nabla \cdot \boldsymbol{u} = 0, \tag{1a}$$

$$\frac{\partial \boldsymbol{u}}{\partial t} = \boldsymbol{u} \times \boldsymbol{\omega} - \nabla\left(\frac{p}{\rho_f} + \frac{\boldsymbol{u}^2}{2}\right) + \nu\nabla^2\boldsymbol{u} + \boldsymbol{f}_F + \boldsymbol{f}_P. \tag{1b}$$

Here, $\boldsymbol{u}$ and $\boldsymbol{\omega}$ are the fluid velocity and vorticity, respectively. p is the pressure, ρ_f is the fluid density, and ν is the kinematic viscosity. The small wave-number forcing term $\boldsymbol{f}_F$ is used to maintain the turbulence with an approximately constant kinetic energy. As suggested in Refs. [29,30], we assume the forcing vector to be proportional to the fluid velocity and added to wave numbers with magnitude $k < 5$. $\boldsymbol{f}_P$ is the particle body force, which is calculated at each Cartesian grid node i using $\boldsymbol{f}_p(\boldsymbol{x}_i) = -\sum_{n=1}^{N} \boldsymbol{F}_n^F \delta_h(\boldsymbol{x}_i - \boldsymbol{X}_{p,n})$. Here, $\boldsymbol{x}_i$ is the location of grid node i, $\boldsymbol{F}_n^F$ is the fluid force on particle n located at $\boldsymbol{X}_{p,n}$, and $\delta_h(\boldsymbol{x}_i - \boldsymbol{X}_{p,n})$ is a regularized δ function. The influence of the particle phase on the flow phase has a non-negligible effect on the agglomeration even when the particle volume fraction $\phi < 0.001$. Since we also consider interactions between particles, our simulation is four-way coupled [5].

It should be noted that all the equations and variables in our simulation have been nondimensionalized by choosing typical length, velocity, and mass scales that are relevant to the agglomeration of solid microparticles. The typical length scale is set as $L_0 = 100 r_p = 0.01$ m, where $r_p = 10\,\mu$m is the particle radius. The typical velocity is $U_0 = 10$ m/s and the typical mass is

$M_0 = \rho_f L_0^3 = 10^{-9}$ kg, where $\rho_f = 1\,\mathrm{kg/m^3}$ is the fluid density. The typical timescale is given by $T_0 = L_0/U_0$. Other dimensional input parameters are the fluid viscosity $\mu = 1.0 \times 10^{-5}$ Pa s, the particle density $\rho_p = 10$–$320\,\mathrm{kg/m^3}$, and the surface energy $\gamma = 0.01$–$5\,\mathrm{J/m^2}$. Hereinafter, all the variables appear in their dimensionless form and, for simplicity, we use the same notations as the dimensional variables.

Before the particles are added into the domain, a preliminary computation is conducted for 5000 time steps with $dt_F = 0.005$ (dimensionless) to allow the turbulence to reach a statistically stationary state. The turbulence kinetic energy q and dissipation rate ϵ are obtained from integration of the power spectrum $E(k)$,

$$q = \int_0^{k_{\max}} E(k)dk, \quad \epsilon = 2\nu \int_0^{k_{\max}} k^2 E(k)dk. \tag{2}$$

2. Solid phase: Adhesive discrete element method

We use the discrete element method (DEM) to model the particles' motion in turbulent flows, which solves the linear and angular momentum equations of particles

$$m_i \dot{\boldsymbol{v}}_i = \boldsymbol{F}_i^F + \boldsymbol{F}_i^C, \tag{3a}$$

$$I_i \dot{\boldsymbol{\Omega}}_i = \boldsymbol{M}_i^F + \boldsymbol{M}_i^C, \tag{3b}$$

where m_i and I_i are mass and moment of inertia of particle i and $\boldsymbol{v}_i$ and $\boldsymbol{\Omega}_i$ are the translational velocity and the rotation rate of the particle. The forces and torques are induced by both the fluid flow ($\boldsymbol{F}_i^F$ and $\boldsymbol{M}_i^F$) and the interparticle contact ($\boldsymbol{F}_i^C$ and $\boldsymbol{M}_i^C$). In this work, the dominant fluid force is the Stokes drag given by

$$\boldsymbol{F}^{\mathrm{drag}} = -3\pi\mu d_p(\boldsymbol{v} - \boldsymbol{u})f, \tag{4a}$$

$$\boldsymbol{M}^{\mathrm{drag}} = -\pi\mu d_p^3\left(\boldsymbol{\Omega} - \tfrac{1}{2}\boldsymbol{\omega}\right), \tag{4b}$$

where $\boldsymbol{u}$, $\boldsymbol{\omega}$, and μ are velocity, vorticity, and viscosity of the fluid and $\boldsymbol{v}$ and d_p are the velocity and the diameter of particles. The friction factor f, given by Ref. [31], is used to correct for the crowding of particles. For particle Reynolds number in the range 0.01 to 10^4, f can be written as

$$f = (1-\phi)^{1-\zeta}, \quad \zeta = 3.7 - 0.65\exp\left[-\tfrac{1}{2}(1.5 - \ln \mathrm{Re}_p)^2\right]. \tag{5}$$

The particle Reynolds number Re_p is defined as $\mathrm{Re}_p = d_p|\boldsymbol{v} - \boldsymbol{u}|/\nu$. In addition to the Stokes drag, we also include the Saffman and Magnus lift forces in $\boldsymbol{F}_i^F$ [32,33].

When two particles i and j are in contact, the normal force F^N, the sliding friction F^S, the twisting torque M^T, and the rolling torque M^R acting on particle i from particle j can be expressed as

$$F_{ij}^N = F_{ij}^{NE} + F_{ij}^{ND} = -4F_C\left(\hat{a}_{ij}^3 - \hat{a}_{ij}^{3/2}\right) - \eta_N \boldsymbol{v}_{ij}\cdot\boldsymbol{n}_{ij}, \tag{6a}$$

$$F_{ij}^S = -\min\left[k_T\int_{t_0}^{t}\boldsymbol{v}_{ij}(\tau)\cdot\boldsymbol{\xi}_S d\tau + \eta_T\boldsymbol{v}_{ij}\cdot\boldsymbol{\xi}_S,\ F_{ij,\mathrm{crit}}^S\right], \tag{6b}$$

$$M_{ij}^T = -\min\left[\frac{k_T a^2}{2}\int_{t_0}^{t}\boldsymbol{\Omega}_{ij}^T(\tau)\cdot\boldsymbol{n}_{ij}d\tau + \frac{\eta_T a^2}{2}\boldsymbol{\Omega}_{ij}^T\cdot\boldsymbol{n}_{ij},\ M_{ij,\mathrm{crit}}^T\right], \tag{6c}$$

$$M_{ij}^R = -\min\left[4F_C\hat{a}_{ij}^{3/2}\int_{t_0}^{t}\boldsymbol{v}_{ij}^L(\tau)\cdot\boldsymbol{t}_R d\tau + \eta_R\boldsymbol{v}_{ij}^L\cdot\boldsymbol{t}_R,\ M_{ij,\mathrm{crit}}^R\right]. \tag{6d}$$

The normal force F_{ij}^N contains an elastic term F_{ij}^{NE} derived from the Johnson-Kendall-Roberts (JKR) contact theory. F_{ij}^{NE} combines the effects of van der Waals attraction and the elastic

deformation and its scale is set by the critical pull-off force, $F_C = 3\pi R_{ij}\gamma$, where $R_{ij} = (r_{p,i}^{-1} + r_{p,j}^{-1})^{-1}$ is the reduced particle radius and γ is the surface energy of the particle. The dimensionless variable $\hat{a}_{ij}$ is calculated by normalizing the radius of the contact region a_{ij} by its value at the zero-load equilibrium state $a_{ij,0}$, expressed as $a_{ij,0} = (9\pi\gamma R_{ij}^2/E_{ij})^{1/3}$ [25], where E_{ij} is the effective elastic modulus. In DEM, $\hat{a}_{ij}$ is calculated inversely from the normal particle overlap, δ, through

$$\frac{\delta}{\delta_C} = 6^{\frac{1}{3}}\left[2(\hat{a}_{ij})^2 - \frac{4}{3}(\hat{a}_{ij})^{\frac{1}{2}}\right], \tag{7}$$

where $\delta_C = a_{ij,0}^2/[2(6)^{1/3}R_{ij}]$ is the critical overlap. The bond between two contacting particles will break when $\delta < -\delta_C$. The sliding friction F^S, twisting torque M^T, and rolling torque M^R [Eqs. (6b)–(6d)] are all calculated using spring-dashpot-slider models, where $\boldsymbol{v}_{ij}\cdot\boldsymbol{\xi}_S$, $\boldsymbol{\Omega}_{ij}^T$, and $\boldsymbol{v}_{ij}^L$ are the relative sliding, twisting, and rolling velocities. k_T in Eq. (6) is the tangential stiffness. The second terms of Eqs. (6a)–(6d) are the viscoelastic damping forces, which are proportional to the rate of motions in each of the respective directions, and η_N, η_T, and η_R are the dissipation coefficients for relative compression, sliding, and rolling motions. The normal dissipation coefficient η_N is calculated as $\eta_N = 2\alpha\sqrt{m_{ij}a_{ij}E_{ij}/3}$, where $m_{ij} = (m_i + m_j)^{-1}$ is the effective mass of two colliding particles with mass m_i and m_j. For details, see Refs. [25,34].

When these resistances reach their critical limits, $F_{ij,\mathrm{crit}}^S$, $M_{ij,\mathrm{crit}}^T$, or $M_{ij,\mathrm{crit}}^R$, a particle will irreversibly slide, twist, or roll relative to its neighboring particle. The critical limits are expressed as [25]

$$F_{ij,\mathrm{crit}}^S = \mu F_C\left|4\left(\hat{a}_{ij}^3 - \hat{a}_{ij}^{3/2}\right) + 2\right|, \tag{8a}$$

$$M_{ij,\mathrm{crit}}^T = \frac{3\pi a_{ij}F_{ij,\mathrm{crit}}^S}{16}, \tag{8b}$$

$$M_{ij,\mathrm{crit}}^R = 4F_C\hat{a}_{ij}^{3/2}\theta_{\mathrm{crit}}R_{ij}. \tag{8c}$$

Here $\mu(=0.3)$ is the friction coefficient and $\theta_{\mathrm{crit}}(=0.01)$ is the critical rolling angle. We set these values according to experimental measurements [35]. The adhesive DEM has been validated by a series of experimental measurements. The details of these validations and the determination of the value of parameters in DEM can be found in Refs. [34,36].

The scales of the elastic term F_{ij}^{NE} in Eq. (6a) and the critical force and torques in Eq. (8) are all in proportion to the surface energy γ, which is the work required to separate two touching surfaces per unit area. An adhesion parameter Ad, which is defined as the ratio between γ and the kinetic energy of particles (per unit area), can be used to quantify the effect of adhesion. Ad is expressed as [23,34,37]

$$\mathrm{Ad} = \frac{\gamma}{\rho_p U^2 r_p}. \tag{9}$$

In this equation, U is the characteristic velocity scale of particles. For particles transported in turbulence, we simply set U equal to the root-mean-square turbulent fluctuation velocity u'. An alternative choice of the velocity scale is discussed in Sec. III E. For large values of the adhesion parameter, particles tend to stick together upon collision, forming particle agglomerates. In contrast, colliding particles tend to rebound from each other when Ad is small. This adhesion parameter has been successfully used to estimate the critical sticking velocity of two colliding particles [38] and predict the packing structure of adhesive particles [22,39,40].

It is known that the fluid squeeze film between particles near contact significantly reduces the approach velocity and further influences the collision and agglomeration process. In this work, viscous damping force derived from the classical lubrication theory is also included, given by

$$F_l = -\frac{3\pi\mu r_p^2}{2h}\frac{dh}{dt}. \tag{10}$$

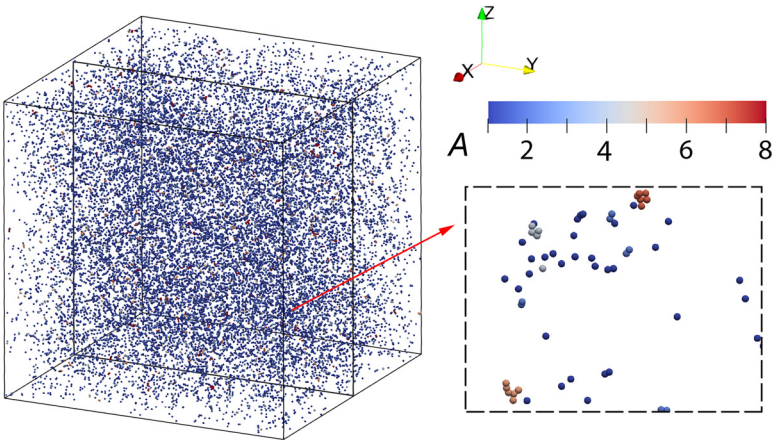

FIG. 1. Snapshot of the simulated system at $t = 20$. The enlarged view from the middle slice ($x = 0$) shows agglomerates and their size A (defined as the number of primary particles contained in the agglomerate, indicated by the color code).

F_l is initiated at surface separation distance $h = 0.01 r_p$ and a minimum value $h = 2 \times 10^{-4} r_p$ is set at the instant of particle contact according to experiments [41,42].

3. Multiple-time step framework

Our DNS-DEM computational framework is designed with multiple-time steps [23,25,37]. The flow field is updated using a fluid time step $dt_F = 0.005$. To correctly identify interparticle collisions, a smaller particle convective time step $dt_P = 2.5 \times 10^{-4}$ is adopted to update the force, velocity, and position of particles that do not collide with other particles. Such a small dt_p ensures that the distance each particle travels during a time step is only a small fraction of the particle or the grid size. In addition, we build a local list at each fluid step to record the neighboring particles that each particle may collide as it is advected over a fluid time step. Once a particle is found to collide with other particles during a particle time step, we then recover its information (i.e., its force, velocity, and position) to the start of this particle time step and instead advect it using a collision time step $dt_C = 6.25 \times 10^{-6}$. The value of dt_C is small enough to resolve the rapid variation of contacting forces, velocity, and position of the particles.

B. Simulation conditions

The system studied in this work is illustrated in Fig. 1. We consider $N = 4 \times 10^4$ non-Brownian solid particles suspended in the homogeneous isotropic turbulent flow in the absence of gravity. The triply periodic computational domain has a dimension of $(2\pi)^3$ with 128^3 grid points. The Taylor Reynolds number is fixed as $\mathrm{Re}_\lambda = 93.0$ in this work. Similar values of Re_λ have also been used in previous studies involving particle-laden flows [12,43,44]. By setting this value of Re_λ, we can easily compare our results with those in literature. Other dimensionless flow parameters, including the fluctuating velocity u', the dissipation rate ϵ, the kinematic viscosity ν, Kolmogorov length η, Kolmogorov time τ_k, and the large-eddy turnover time T_e, are listed in Table I.

The particle radius is fixed as $r_p = 0.01$. We choose the value of particle radius so that the particle size and the Kolmogorov length scale are comparable. We choose this relatively large value of particle size to increase the collision rates, which helps ensure good statistics on agglomeration within a feasible computing time. The particle volume concentration is $\phi = \frac{4N\pi r_p^3}{3(2\pi)^3} = 6.8 \times 10^{-4}$, which is small so that the system can be regarded as a dilute system. The fluid density ρ_f is set as 1 (nondimensional), and five different values (10, 40, 80, 160, and 320) are used as particle density

TABLE I. Dimensionless parameters of the fluid turbulence, including the fluctuating velocity u', the dissipation rate ϵ, the kinematic viscosity ν, Taylor-microscale Reynolds number Re_λ, Kolmogorov length η, Kolmogorov time τ_k, and the large-eddy turnover time T_e.

u'	ϵ	ν	Re_λ	η	τ_k	T_e
0.28	0.0105	0.001	93.0	0.0175	0.31	7.4

ρ_p to achieve different values of particle response time. We have neglected the influence of gravity in the present study since it does not play an important role in the agglomeration of particles with radius less than 40 μm [45]. For detailed discussions on the effect of gravity on collision rate for large particles (with size above 40 μm), we refer to Refs. [46,47].

One of the most important parameters governing the agglomeration is the Kolmogorov-scale Stokes number, $\mathrm{St_k} = \tau_p/\tau_k$, where $\tau_p = m/(6\pi r_p \mu)$ is the particle response time and $\tau_k = (\nu/\epsilon)^{1/2}$ is the Kolmogorov time. In the classical theory of turbulent collision of nonadhesive particles, $\mathrm{St_k}$ significantly influences the value of the collision kernel. In the presence of adhesion, the adhesion parameter $\mathrm{Ad} = \gamma/(\rho_p u'^2 r_p)$ is used to quantify the adhesion effect [23]. The particle surface energy γ can be determined according to experimental measurements [35,48] or calculated from the Hamaker coefficients of the materials [23]. In this work, we systematically vary Ad (by varying γ) in a wide range at five different $\mathrm{St_k}$ values (0.72, 2.9, 5.8, 12, and 23) to show the effect of adhesion on the agglomeration.

C. Smoluchowski's theory

Before showing the DNS-DEM results, we introduce the Smoluchowski coagulation equation and discuss how to apply the theory to the agglomeration of noncoalescing adhesive particles. In Smoluchowski's theory, the growth of agglomerates can be described using the population balance equation (PBE) [6]

$$\dot{n}(A) = \frac{1}{2}\sum_{i+j=A} \Gamma(i,j)n(i)n(j) - n(A)\sum_{i=1}^{\infty} \Gamma(i,A)n(i), \tag{11}$$

where $\Gamma(i,j)$ is the averaged rate constant (kernel) for agglomerates of size i colliding with agglomerates of size j and should reflect all the factors affecting agglomeration. It is defined as $\Gamma(i,j) \equiv \dot{n}_{c,ij}/[n(i)n(j)]$ with $\dot{n}_{c,ij}$ being the collision rate per unit volume and $n(i)$ being the average number concentration of size group i. The first term on the right-hand side of Eq. (11) is the source term that accounts for the rate at which agglomerates of size A are created. The second term is a sink that describes agglomerate disappearance due to its coalescence with other agglomerates.

PBE can be readily used to predict the growth of droplets in clouds with an underlying assumption—colliding particles coalesce instantaneously to form larger particles [49]. Therefore, the growth rate of agglomerates is equivalent to the collision rate. The collision between adhesive noncoalescing microparticles, however, does not ensure the growth of an agglomerate. Both sticking and rebound could happen as a result of the competition between the particles' kinetic energy and the surface energy. Thus, it is natural to introduce a sticking probability, Θ, defined as the ratio of the number of collisions that lead to agglomeration to the total number of collisions. We then have an *agglomeration kernel*, which reads

$$\Gamma_a(i,j) = \Theta\Gamma(i,j), \ \forall i,j. \tag{12}$$

The sticking probability has a minimum value 0 for nonadhesive particle systems and a maximum value 1, corresponding to the hit-and-stick case in conventional PBE simulations. We can then simulate the agglomeration with different adhesion level, by simply replacing $\Gamma(i,j)$ in Eq. (11) by

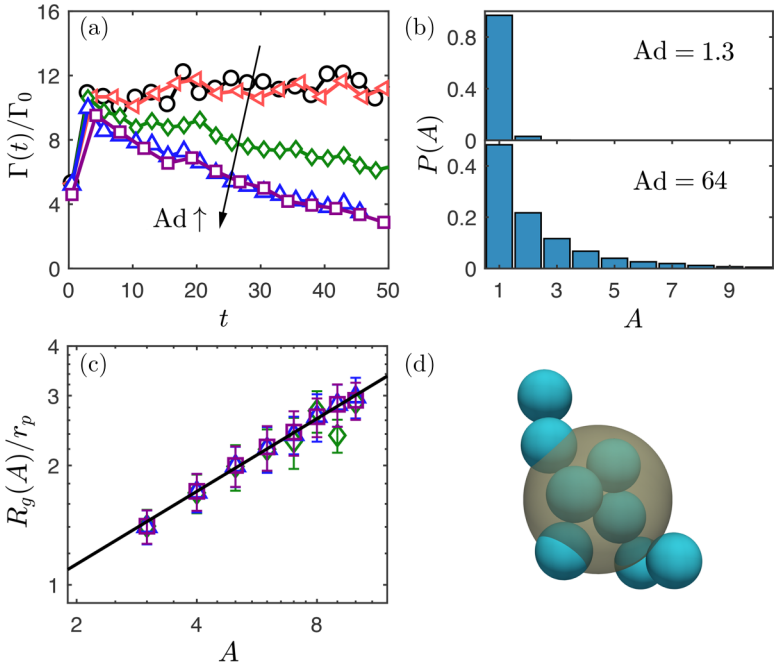

FIG. 2. (a) Temporal evolution of the collision kernel $\Gamma(t)/\Gamma_0$ for cases with $\mathrm{St_k} = 5.8$ and $\mathrm{Ad} = 0.013$ (circles), 1.3 (left-pointing triangles), 13 (diamonds), 64 (upward triangles), and 128 (squares). (b) Fraction of particles, $P(A)$, contained in agglomerates of size A at $t = 15$ for $\mathrm{Ad} = 1.3$ and 64. (c) Gyration radius of agglomerates $R_g(A)/r_p$ as a function of agglomerate size A at $t = 15$ for the cases with $\mathrm{St_k} = 5.8$ and $\mathrm{Ad} = 13$ (diamonds), 64 (triangles), and 128 (squares). The solid line shows Eq. (13) with $\chi = 1.64$ and $D_f = 1.64$. (d) An agglomerate produced in the simulation with $\mathrm{St} = 5.8$ and $\mathrm{Ad} = 64$ with its equivalent sphere with radius of gyration (shaded region).

$\Gamma_a(i, j)$. We will show below that such simple modification can well reproduce DNS-DEM results in a statistical manner.

The structure of agglomerates is another crucial factor affecting the agglomeration rate. For noncoalescing adhesive particles, the formed agglomerates usually have fractal structures, which distinguishes our system from those of droplets [26,50]. In systems involving Brownian nanoparticles, theoretical collision kernels can be extended to fractal agglomerates when substituting the particle radius with the radius of effective collision spheres (ECSs) for an agglomerate [51,52]. We will show below that the idea of the effective radius can also be applied to non-Brownian inertial particles.

III. RESULTS AND DISCUSSIONS

A. Collision rate, agglomerate size, and structure

We first measure the temporal evolution of the collision kernel in a system with $\mathrm{St_k} = 5.8$ and Ad varying from 0.013 to 128. To show the effect of adhesion, here we simply regard the system as a monodisperse system and count the collisions between every primary particle. The effective collision kernel is then calculated as $\Gamma = 2\dot{n}_c/n_0^2$, where n_0 is the number density of primary particles. The temporal evolution of the collision kernel $\Gamma(t)$, normalized by the collision kernel for zero-inertia particles $\Gamma_0 = (8\pi\epsilon/15\nu)^{1/2}(2r_p)^3$ [9], is shown in Fig. 2(a). When the adhesion is extremely weak ($\mathrm{Ad} = 0.013$ and 1.3), the collision kernel rapidly reaches a statistically steady state with $\Gamma(t)/\Gamma_0 = 11.1$. This value is quite close to the previous DNS results for nonadhesive particles with the same inertia [12]. As Ad increases, the collision kernel is significantly reduced

and the system is pushed away from equilibrium. Since adhesion number only affects the interaction between contacting particles, we attribute these phenomena to adhesion-enhanced agglomeration. When Ad is larger than 64, further increase of Ad does not change the curve of collision kernel because in this strong-adhesion limit, the sticking probability for colliding particles is essentially unity and every collision event will lead to agglomeration. The overall collision kernel is determined by the size distribution of the agglomerates in the system, which is mainly determined by the turbulent transport and is insensitive to the adhesion in this large Ad limit.

In Fig. 2(b), the agglomeration at $t = 15$ is clearly displayed in the form of the fraction of particles $P(A)$ contained in an agglomerate of size A. The agglomerate size A is defined as the number of primary particles contained in that agglomerate. For small Ad, most particles remain as singlets ($A = 1$) and only a small number of particles ($\sim$4%) are contained in agglomerates of size $A \geqslant 2$. In contrast, cases with large Ad yield a considerable number of agglomerates with size A up to 20.

To model the agglomeration process in the framework of Smoluchowski's equation, a measure of agglomerate structure in the form of the equivalent sphere is necessary. One such quantity is the radius of gyration, defined for an agglomerate with 3 or more primary particles ($A \geqslant 3$) by $R_g(A) = (\Sigma_1^A |\boldsymbol{X}_i - \bar{\boldsymbol{X}}_i|^2/A)^{1/2}$, where $\boldsymbol{X}_i$ denotes the position of ith particle within the agglomerate and $\bar{\boldsymbol{X}}_i$ is the center of mass of the agglomerate. For agglomerates with two primary particles, we use the explicit expression $R_g(2) = \sqrt{1.6} r_p$ suggested in Ref. [53].

In Fig. 2(d), we show an agglomerate generated from DNS-DEM simulation and its equivalent sphere with the radius of gyration. We calculate R_g for all the agglomerates produced in the simulations in Fig. 2(a) at $t = 15$ and plot the ratio R_g/r_p as a function of agglomerate size A in Fig. 2(c) (large size agglomerates with $A > 12$ only contain 0.2% particles and thus are neglected here). The results fall onto a power-law curve

$$\frac{R_g(A)}{r_p} = \left(\frac{A}{\chi}\right)^{\frac{1}{D_f}}, \quad \text{for } A > 2, \tag{13}$$

with the factor $\chi = 1.64$ and the fractal dimension $D_f = 1.64$. The D_f value measured here is consistent with experimental measurements of Waldner *et al.* [53], who measured the radius of gyration for early-stage agglomerates formed in a stirred tank using small angle static light scattering [53]. The value of fractal dimension fitted from experimental results is $D_f = 1.7 \pm 0.1$, which is consistent with results of our simulations. Selomulya *et al.* adopted the same experimental technique to measure the shear-induced agglomeration of latex particles and reported values of D_f between 1.7 and 2.1 [54]. Their results are close to but slightly larger than the values of D_f measured in our DNS-DEM results. The possible reason for the deviation is that Selomulya *et al.* assumed the factor χ to be 1.01 in their measurements. Such a small value of χ may give D_f that is larger than the actual value. It should be noted that we focus on the agglomeration at an early stage in the current study, when the restructuring and breakage of agglomerates are normally not involved [53]. These phenomena will lead to a variation of factor χ and the fractal dimension D_f [55], which is left for future work.

B. Effect of Stokes number

The temporal evolution of the collision kernel $\Gamma(t)/\Gamma_0$, the fraction of particles, $P(A)$, contained in agglomerates of size A, and the gyration radius of agglomerates $R_g(A)/r_p$ for cases with different Stokes number $\mathrm{St_k}$ and adhesion parameter Ad are plotted in Fig. 3. For particles with small inertia ($\mathrm{St_k} = 0.72$), the increase of adhesion parameter only has a limited effect on the temporal evolution of the collision kernel [Fig. 3(a)]. Moreover, there is no obvious statistical steady state for the system with $\mathrm{St_k} = 0.72$. The reason is that the lubrication force between particles near contact significantly reduces the collision rate for particles with small inertia [41] and the collision rate is too small to form a considerable number of agglomerates even if the adhesion is strong. The system thus behaves as a monodisperse system. This is further displayed in the form of the fraction of particles

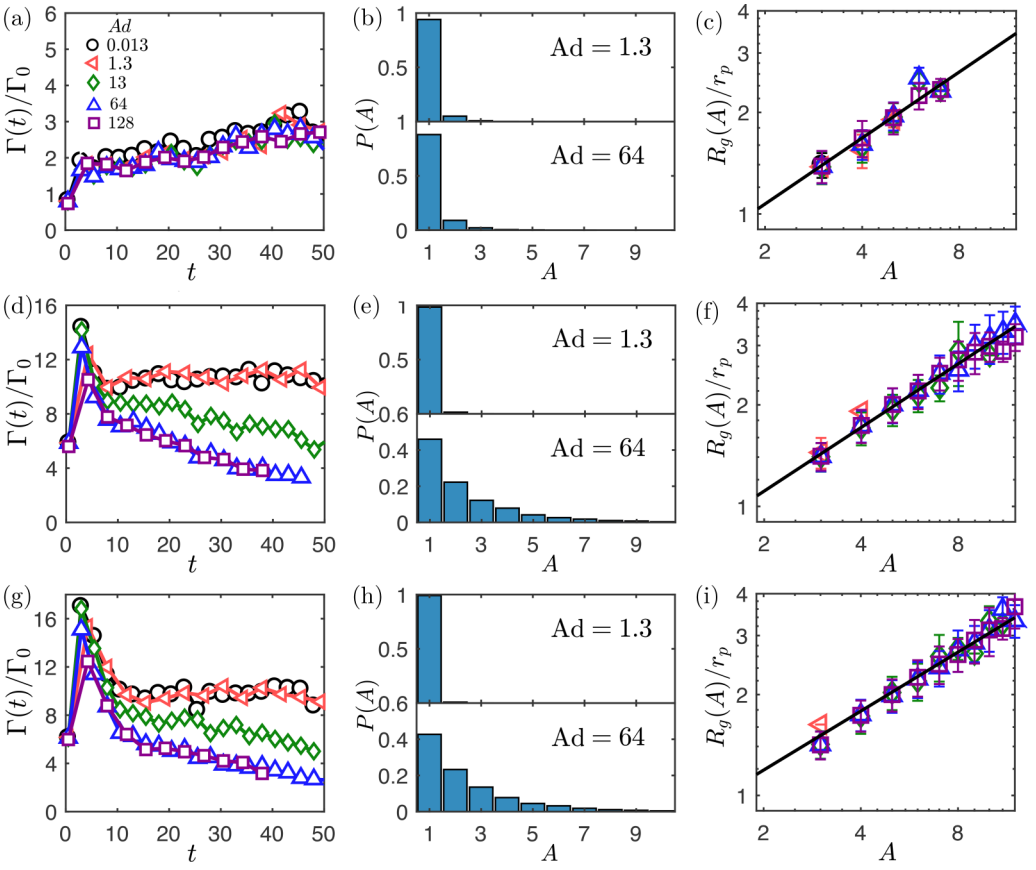

FIG. 3. Left [panels (a), (d), and (g)]: Temporal evolution of the collision kernel $\Gamma(t)/\Gamma_0$. Middle [panels (b), (e), and (h)]: Fraction of particles, $P(A)$, contained in agglomerates of size A at $t = 15$ for Ad = 1.3 and 64. Right [panels (c), (f), and (i)]: Gyration radius of agglomerates $R_g(A)/r_p$ as a function of agglomerate size A at $t = 15$. The solid lines in panels (c), (f), and (i) are fits to Eq. (13) with (c) $\chi = 1.80$ and $D_f = 1.54$, (f) $\chi = 1.70$, $D_f = 1.60$, and (i) $\chi = 1.49$, $D_f = 1.71$. Different rows stand for results for different $\mathrm{St_k}$: top, $\mathrm{St_k} = 0.72$; middle, $\mathrm{St_k} = 12$; and bottom, $\mathrm{St_k} = 23$.

$P(A)$ contained in an agglomerate of size A [Fig. 3(b)]. In both strong and weak adhesion cases, most particles remain as singlets.

For particles with higher Stokes number, $\mathrm{St_k} = 12$ or 23, similar results are observed as those for $\mathrm{St_k} = 5.8$ in Fig. 2. In both cases, a statistical steady state can be identified in the temporal evolution of the collision kernel $\Gamma(t)/\Gamma_0$ at the small Ad limit [Figs. 3(d) and 3(g)]. When Ad > 64, further increase of Ad does not change the $\Gamma(t)/\Gamma_0 - t$ curves. The results once again confirm the existence of the strong adhesion limit. In this limit, one can simply adopt the hit-and-stick assumption—two particles will stick together once there is a contact between them—to simulate the agglomeration without performing DEM calculations. In Figs. 3(e) and 3(h), we observe similar results as those for $\mathrm{St_k} = 5.8$ in Fig. 2(b).

For all the three values of $\mathrm{St_k}$, the radius of gyration for agglomerates of different size can be well described using the power-law function in Eq. (13) [see Figs. 3(c), 3(f), and 3(i)]. For a given $\mathrm{St_k}$, the factor χ and fractal dimension D_f are insensitive to the value of adhesion parameter Ad. It suggests that the interparticle adhesion strongly affects the growth rate of early-stage agglomerates but have no obvious impact on their structures. Interestingly, as we mentioned in the previous subsection, the agglomerates formed in different experimental conditions also have similar values of D_f, which

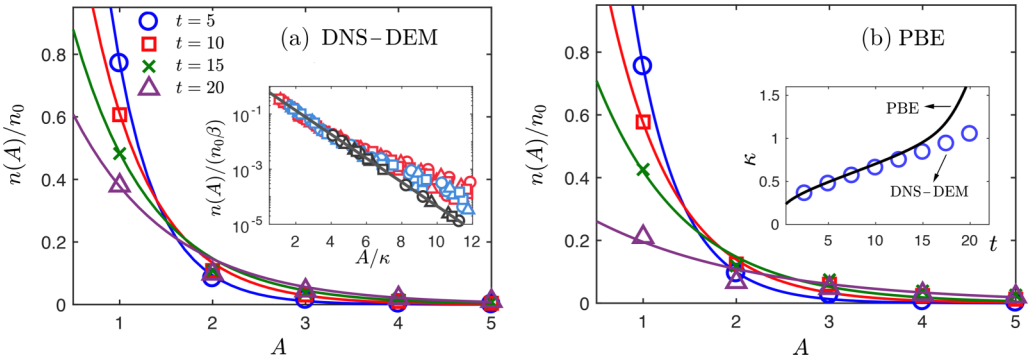

FIG. 4. (a) Scaled number density $n(A)/n_0$ of agglomerates of size A for the case with $\mathrm{St_k} = 5.8$ and $\mathrm{Ad} = 64$ at $t = 5$ (circles), 10 (squares), 15 (crosses), and 20 (triangles). The solid lines are fits to Eq. (14). Inset: scaled number density $n(A)/(n_0\beta)$ as a function of A/κ for $\mathrm{St_k} = 5.8$ (circles), 12 (triangles), and 23 (squares). For each $\mathrm{St_k}$, results are shown for $\mathrm{Ad} = 1.3$ (black), 13 (blue), and 64 (red), at $t = 5$, 10, and 15. The solid line is the exponential scaling $y = \exp(-x)$. (b) $n(A)/n_0$ vs A calculated from population balance equations. Legends are the same as in panel (a). In the inset of panel (b), we show the temporal evolution of the scale parameter κ from DNS-DEM result (circles) and from PBE (solid line).

further implies that the influences of flow conditions and interparticle adhesion on the structure of agglomerates may be significant only if the size of agglomerates is sufficiently large [55].

C. Exponential scaling of early stage agglomerate size

Figure 4(a) shows the distributions of number density of agglomerates as a function of size A at early stage ($t \leqslant 20$). These distributions, when scaled by the initial number density of primary particles n_0, follow an exponential equation [solid lines in Fig. 4(a)],

$$\frac{n(A)}{n_0} = \beta \exp\left(-\frac{A}{\kappa}\right), \tag{14}$$

with the coefficients β and κ depending on time. Based on the conservation of the total number of primary particles, $\Sigma_1^\infty An(A) = n_0$, the prefactor β can be expressed as $\beta(\kappa) = 2\cosh(\kappa^{-1}) - 2$. Therefore, the size distribution of early-stage agglomerates is determined by a single scale parameter κ, which gives a typical value of the size of agglomerates. A larger value of κ means that there are more particles contained in agglomerates with larger size and the growth of early-stage agglomerates can be characterized by the increase of κ. In the inset of Fig. 4(a), the number density distributions for cases with $\mathrm{St_k} = 5.8$, 12, and 23 and $\mathrm{Ad} = 1.3$, 13, and 64 are plotted in a rescaled form, $n(A)/(n_0\beta) \sim A/\kappa$. Except for the deviation in tail caused by agglomerates with $n(A)/n_0 < 0.3\%$, the results center around the curve $y = \exp(-x)$, suggesting that the exponential scaling for early-stage agglomeration is valid for inertial particles across a wide range of adhesion force magnitudes.

A comparison between the exponential distribution and the well-known self-preserving size distribution for Brownian nanoparticles [56–58] would be of interest. If the collision kernels are homogeneous functions of the volume of colliding particles and the degree of homogeneity smaller than unity, the particle size distribution will reach a self-preserving shape (normally bell-shaped). In that case, tracking the evolution of the mean agglomerate size is sufficient to describe the growth of agglomerates. Although both the exponential distribution in Eq. (14) and the self-preserving size distribution are single-parameter distributions, there is a fundamental difference between them. The exponential distribution describes the transition behavior at the early stage of the agglomeration when most particles remain as singlets and is no longer valid when there is a considerable number of large agglomerates. In contrast, the self-preserving size distribution is an asymptotic limit which is invariant with time.

Now we introduce how to construct the agglomeration kernel that can be applied to Smoluchowski's theory based on DNS-DEM results. We first look at the strong adhesion case by assuming that particles will stick together upon collisions (i.e., $\Theta = 1$) and then show how adhesion influences the sticking probability. For spherical particles, $\Gamma(i, j)$ can be modeled by [13]

$$\Gamma(i, j) = 2\pi R_{ij}^2 \langle |w_r| \rangle g(R_{ij}), \tag{15}$$

where $R_{ij} = r_{p,i} + r_{p,j}$ is the collision radius, $\langle |w_r| \rangle$ is the average radial relative velocity and $g(R_{ij})$ is the radial distribution function at contact. Explicit expressions of these quantities are summarized in Ref. [13]. Since turbulence parameters are fixed here, R_{ij}, $\langle w_r \rangle$, and $g(R_{ij})$ are determined by particle size and $\mathrm{St_k}$. For collisions between agglomerates, we simply use the radius of gyration in Eq. (13) with known values of χ and D_f instead of the particle radius r_p to calculate all the quantities in Eq. (15) [51,59,60]. For instance, the collision radius for an agglomerate with i primary particles and that with j primary particles is calculated as $R_{ij} = R_g(i) + R_g(j)$. The gyration radius $R_g(i)$ is given by Eq. (13) when $i > 2$ and $R_g(i) = r_p$ and $\sqrt{1.6} r_p$ for $i = 1$ and $i = 2$, respectively. Given the initial conditions, $n(1) = n_0$ and $n(i) = 0$ for $i > 1$, PBEs in Eq. (11) are numerically integrated using a sufficiently small time step with the agglomerate size truncated at $i_C = 50$ (i.e., assuming $n(i) = 0$ for $i > 50$). As a result, we can get the evolution of the number density $n(i)$ for each size group. PBE calculations are much faster than DNS-DEM, since PBEs only solve for the number density $n(i)$ at each time step rather than resolve the motion of every particle.

We plot the scaled number density $n(A)/n_0$ calculated from PBE in Fig. 4(b). It is shown that results from PBE well reproduce the results of DNS-DEM in Fig. 4(a) when $t \leqslant 15$. We then fit the scaled distribution $n(A)/n_0$ using the Eq. (14) at each t and get the evolution of the scale parameter κ, which is in good agreement with the DNS results when $t \leqslant 15$ [see the inset of Fig. 4(b)]. It indicates that the kernel $\Gamma(i, j)$ constructed in the form of gyration radius readily reflects the effect of the fractal structure of agglomerates on the agglomeration. At $t = 20$, the distribution of $n(A)/n_0$ from PBE still follows the exponential form; however, a non-negligible deviation between PBE results and those from DNS-DEM is observed. Such deviation may be attributed to two reasons. First, $\Gamma(i, j)$ does not contain information of breakage or rearrangement, which is expected to be significant for large-size agglomerates [26]. Moreover, statistics may also get worse when the total number of agglomerates $\Sigma_1^\infty n(A)$ reduces.

D. Effect of adhesion on growth of agglomerates

When the adhesion is relatively weak, a collision between two particles or agglomerates does not ensure the formation of a larger agglomerate. The adhesive DEM approach can capture the effect of adhesion on the agglomeration without any additional models. However, when designing large-scale devices, one does not need to know the information of every single particle; instead, knowing the size distribution is enough. In those cases, solving the population balance equations would be more feasible. Therefore, it is of significance to check if the complicated effect of particle-particle contacting interactions on the growth kinetics of agglomerates can be captured by the sticking probability Θ [given in Eq. (12)].

We solve PBE using agglomeration kernel $\Gamma_a(i, j)$ with Θ increasing from 0 to 1 [see Eq. (12)]. The evolution of the scale parameter κ is shown as solid lines in Fig. 5(a). It is evident from the results that a smaller sticking probability Θ leads to a lower growth rate of agglomerates. We also plot corresponding results from DNS-DEM simulations with different values of adhesion parameter Ad as data points in Fig. 5(a). For $\mathrm{Ad} = 0.013$, $\kappa(t)$ is close to the PBE results with sticking probability $\Theta = 0$, indicating that almost no agglomerates are formed given such a weak adhesive force. As Ad increases beyond ~64, the $\kappa(t)$ curves converge to the PBE result with sticking probability $\Theta = 1$. This strong adhesion case corresponds to the conventional PBE simulations, where the hit-and-stick assumption is made. Our results here suggest that PBE can also simulate the agglomeration process for particles with relatively weak adhesion once the sticking probability Θ is adopted.

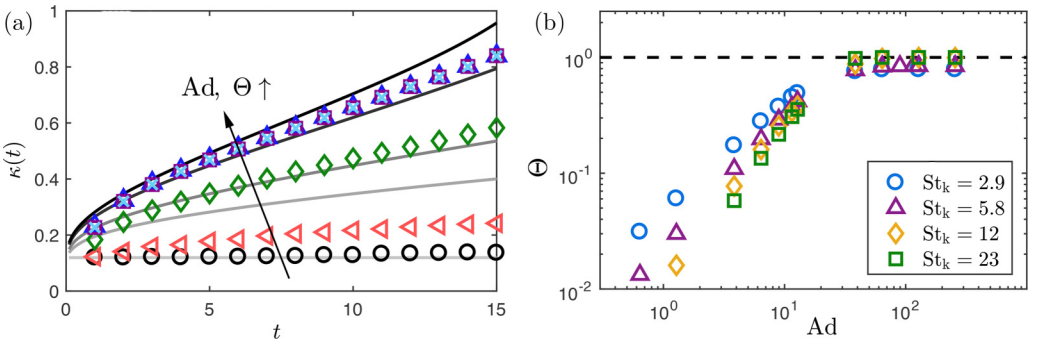

FIG. 5. (a) Temporal evolution of the parameter κ for DNS-DEM simulation with $\mathrm{St_k} = 5.8$ and $\mathrm{Ad} = 0.013$ (circles), 1.3 (left-pointing triangles), 13 (diamonds), 64 (upward triangles), 128 (squares), and 256 (axes). The solid lines spanning from light to dark color are results from PBE with the sticking probability $\Theta = 0$, 0.2, 0.4, 0.8, and 1. (b) Sticking probability Θ, determined from Eq. (16), as a function of adhesion parameter Ad for $\mathrm{St_k} = 2.9$ (circles), 5.8 (triangles), 12 (diamonds), and 23 (squares). The horizontal dashed line is $\Theta = 1$.

We then determine the value of the sticking probability Θ in a statistical manner based on our DNS-DEM data. For a given Ad, we extract the instantaneous value of the scaling parameter $\kappa(t, \mathrm{Ad})$ from DNS-DEM simulations, map this point out on Fig. 5(a), and find the PBE curve of $\kappa(t, \Theta)$ that the point sits on. This procedure instantaneously correlates $\Theta(t)$ to Ad. Then time averaging is performed to get the sticking probability at this given Ad:

$$\Theta(\mathrm{Ad}) = \frac{1}{T}\int_0^T \Theta(t)dt. \tag{16}$$

In Fig. 5(b), we plot $\Theta(\mathrm{Ad})$ for $\mathrm{St_k} = 2.9$, 5.8, 12, and 23. With $\mathrm{Ad} < 1$, the sticking probability Θ for any $\mathrm{St_k}$ is smaller than $\sim$0.3% and the data points of different $\mathrm{St_k}$ are rather scattered. In contrast, when $\mathrm{Ad} > 10$, there is an adhesion-controlled regime, in which Θ is mainly determined by Ad. Particularly, the probability of unity, $\Theta \approx 1$, which corresponds to the hit-and-stick situation, is achieved when Ad is larger than $\sim$50.

E. Modeling sticking probability Θ

Describing turbulence-induced agglomeration using PBE requires knowledge of the sticking probability Θ *a priori* . Therefore, it is of significance to relate Θ to the particle-level properties. We consider a head-on collision between two primary particles with v_{cn} being the relative collision velocity. For simplicity, only the normal forces in Eq. (6a) are taken into account and the interparticle overlap δ evolves according to

$$\frac{d^2\delta}{dt^2} + \frac{2\eta_N}{m}\frac{d\delta}{dt} + \frac{8F_C}{m}[\hat{a}^3(\delta) - \hat{a}^{3/2}(\delta)] = 0, \tag{17}$$

with the initial conditions $\delta(0) = 0$ and $\frac{d\delta}{dt} = v_{cn}$. The contact between the particles is built up when $\delta > 0$ and is broken when $\delta < -\delta_C$. Normalizing the overlap using its critical value δ_C and the time using δ_C/v_{cn}, we have the following nondimensional form of Eq. (17):

$$\frac{d^2\hat{\delta}}{d\hat{t}^2} + B\alpha\hat{a}^{1/2}\frac{d\hat{\delta}}{d\hat{t}} + 3.63B^2 g(\hat{\delta}) = 0. \tag{18}$$

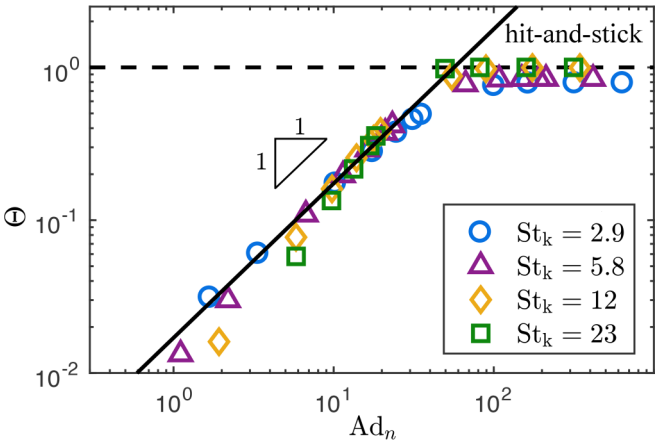

FIG. 6. Sticking probability Θ as a function of the adhesion parameter Ad_n, which is defined based on the averaged normal collision velocity $\langle v_{cn}\rangle$, for $\mathrm{St_k} = 2.9$ (circles), 5.8 (triangles), 12 (diamonds), and 23 (squares). The solid line is $\Theta = 0.017\mathrm{Ad}_n$ and the horizontal dashed line is $\Theta = 1$.

The damping coefficient α is an input parameter and the scaled radius $\hat{a}$ can be calculated inversely through Eq. (7). The results of a collision are determined by the parameter B, which is defined as

$$B = 2.24\left(\frac{E_{ij}}{\rho_p v_{cn}^2}\right)^{-\frac{1}{3}}\left(\frac{\gamma}{\rho_p v_{cn}^2 r_p}\right)^{\frac{5}{6}}. \tag{19}$$

From Eq. (19) and a simple dimensional analysis, it is obvious that the effect of the adhesion (i.e., the surface energy γ) on the sticking probability θ is determined by the dimensionless adhesion parameter $\mathrm{Ad}(v_{cn}) \equiv \gamma/(\rho_p v_{cn}^2 r_p)$, which is defined based on the normal collision velocity v_{cn}. We measure the value of v_{cn} for every collision event in each simulation run and use the mean value $\langle v_{cn}\rangle$ as the typical velocity scale. A modified adhesion parameter then is given as

$$\mathrm{Ad}_n = \frac{\gamma}{\rho_p \langle v_{cn}\rangle^2 r_p}. \tag{20}$$

In Fig. 6, we replot the data of Fig. 5(b) in the $\Theta - \mathrm{Ad}_n$ plane and all the data points collapse onto two curves:

$$\Theta = 0.017\mathrm{Ad}_n, \text{ for } 1 < \mathrm{Ad}_n < 30, \text{ and } \Theta = 1 \text{ for } \mathrm{Ad}_n > 50. \tag{21}$$

The results in Fig. 6 indicate that the mean relative collision velocity is an appropriate choice to scale the effect of adhesion and the sticking probability Θ can be well estimated once Ad_n is known. Here, the data points for cases with $\mathrm{Ad}_n < 1$ are neglected, since the sticking probability is less than 10^{-2}, which is too small to ensure good statistics. It should be noted that current values of $\langle v_{cn}\rangle$ are measured from DNS-DEM. To avoid computationally expensive DNS-DEM calculation, one can also adopt analytical expressions to estimate the value of $\langle v_{cn}\rangle$ (see Refs. [61–64]).

IV. CONCLUSIONS

In summary, for adhesive inertial particles suspended in turbulence, we measure both the collision rate, the structure, and the size distribution of early-stage agglomerates with varying adhesion. We find that the collision rate is significantly reduced due to the adhesion-induced agglomeration. As the value of adhesion parameter Ad increases, the system reaches a strong-adhesion limit, in which the sticking probability for colliding particles is unity and further increase of Ad does not affect the dynamics of agglomeration. We also find that the size distribution of early-stage agglomerates follows

an exponential equation $n(A)/n_0 = \beta(\kappa)\exp(-A/\kappa)$ regardless of the adhesion force magnitude. The transient dynamics of agglomeration at early stages thus can be characterized using a single scale parameter κ. This finding may help to reduce the computing complexity of the population balance equation (PBE) to that of monodisperse systems since only one parameter κ needs to be solved [58]. The evolution of κ then serves as an indicator for the quantitative comparison between DNS-DEM and PBE simulations. We show that by introducing an agglomeration kernel constructed in terms of gyration radius of agglomerates and a sticking probability Θ, PBE can well reproduce the results of DNS-DEM. A relationship between the sticking probability and particle properties is then proposed based on the scaling analysis of the equation for head-on collisions.

There are several interesting directions for future study. First, the current work focuses on the early-stage agglomeration, where the breakage and the rearrangement of agglomerates are not significant. It is unclear to what extent the framework developed here can be extended to situations with large agglomerates [65]. It requires one to construct kernel functions that contain information about breakage and restructuring [66,67]. Moreover, we fix the value of Taylor-microscale Reynolds number Re_λ in the current work. It is reported that the relative velocity and the collision rate for inertial particles increase strongly with increasing Re_λ [12,13,68]. However, a stronger clustering effect may suppress the agglomeration [69]. For high-Reynolds-number flows, other effects, including the correlated collision events [70] and multifractal statistics of velocities differences [71], may dominate the agglomeration. Therefore, a complete picture of agglomeration should include the role of both the turbulent transport (e.g., vortices and intermittency) and the microphysical mechanisms (particle-level interactions), which is an interesting direction for future research.

ACKNOWLEDGMENTS

S.Q.L. acknowledges support from the National Natural Science Foundation of China (Grant No. 51725601) and National Key Research and Development Program of China (Grant No. 2016YFB0600602). The authors thank Prof. Q. Yao at Tsinghua, Prof. L. Mädler at the University of Bremen, and Dr. W. Liu at University of Surrey for useful suggestions.

[1] E. W. Saw, R. A. Shaw, S. Ayyalasomayajula, P. Y. Chuang, and A. Gylfason, Inertial Clustering of Particles in High-Reynolds-Number Turbulence, Phys. Rev. Lett. **100**, 214501 (2008).

[2] J. Lu, H. Nordsiek, E. W. Saw, and R. A. Shaw, Clustering of Charged Inertial Particles in Turbulence, Phys. Rev. Lett. **104**, 184505 (2010).

[3] J. Bec, H. Homann, and S. S. Ray, Gravity-Driven Enhancement of Heavy Particle Clustering in Turbulent Flow, Phys. Rev. Lett. **112**, 184501 (2014).

[4] K. Gustavsson, S. Vajedi, and B. Mehlig, Clustering of Particles Falling in a Turbulent Flow, Phys. Rev. Lett. **112**, 214501 (2014).

[5] S. Balachandar and J. K. Eaton, Turbulent dispersed multiphase flow, Annu. Rev. Fluid Mech. **42**, 111 (2010).

[6] M. Smoluchowski, Versuch einer mathematischen Theorie der Koagulationskinetik kolloider Lösungen, Z. Phys. Chem. **92**, 129 (1917).

[7] S. K. Friedlander, *Smoke, Dust, and Haze: Fundamentals of Aerosol Dynamics* (Oxford University Press, New York, USA, 2000).

[8] A. Pumir and M. Wilkinson, Collisional aggregation due to turbulence, Annu. Rev. Condens. Matter Phys. **7**, 141 (2016).

[9] P. G. F. Saffman and J. S. Turner, On the collision of drops in turbulent clouds, J. Fluid Mech. **1**, 16 (1956).

[10] J. Abrahamson, Collision rates of small particles in a vigorously turbulent fluid, Chem. Eng. Sci. **30**, 1371 (1975).

[11] S. Sundaram and L. R. Collins, Collision statistics in an isotropic particle-laden turbulent suspension. Part 1. Direct numerical simulations, J. Fluid Mech. **335**, 75 (1997).
[12] L. P. Wang, A. S. Wexler, and Y. Zhou, Statistical mechanical description and modelling of turbulent collision of inertial particles, J. Fluid Mech. **415**, 117 (2000).
[13] Y. Zhou, A. S. Wexler, and L. P. Wang, Modelling turbulent collision of bidisperse inertial particles, J. Fluid Mech. **433**, 77 (2001).
[14] K. Gustavsson and B. Mehlig, Statistical model for collisions and recollisions of inertial particles in mixing flows, Eur. Phys. J. E **39**, 55 (2016).
[15] M. Wilkinson and B. Mehlig, Caustics in turbulent aerosols, Europhys. Lett. **71**, 186 (2005).
[16] K. Gustavsson and B. Mehlig, Distribution of relative velocities in turbulent aerosols, Phys. Rev. E **84**, 045304 (2011).
[17] G. Falkovich and A. Pumir, Sling effect in collisions of water droplets in turbulent clouds, J. Atmos. Sci. **64**, 4497 (2007).
[18] A. Jaworek, A. Marchewicz, A. T. Sobczyk, A. Krupa, and T. Czech, Two-stage electrostatic precipitators for the reduction of PM2.5 particle emission, Prog. Energy Combust. Sci. **67**, 206 (2018).
[19] P. Jarvis, B. Jefferson, J. Gregory, and S. A. Parsons, A review of floc strength and breakage, Water Res. **39**, 3121 (2005).
[20] J. Blum, G. Wurm, S. Kempf, T. Poppe, H. Klahr, T. Kozasa, M. Rott, T. Henning, J. Dorschner, R. Schräpler *et al.*, Growth and form of Planetary Seedlings: Results from a Microgravity Aggregation Experiment, Phys. Rev. Lett. **85**, 2426 (2000).
[21] C. Tien, C. S. Wang, and D. T. Barot, Chainlike formation of particle deposits in fluid-particle separation, Science **196**, 983 (1977).
[22] S. Chen, W. Liu, and S. Q. Li, Effect of long-range electrostatic repulsion on pore clogging during microfiltration, Phys. Rev. E **94**, 063108 (2016).
[23] J. S. Marshall and S. Q. Li, *Adhesive Particle Flow* (Cambridge University Press, New York, USA, 2014).
[24] J. Bec, S. Musacchio, and S. S. Ray, Sticky elastic collisions, Phys. Rev. E **87**, 063013 (2013).
[25] J. S. Marshall, Discrete-element modeling of particulate aerosol flows, J. Comput. Phys. **228**, 1541 (2009).
[26] F. F. Dizaji and J. S. Marshall, On the significance of two-way coupling in simulation of turbulent particle agglomeration, Powder Technol. **318**, 83 (2017).
[27] M. Sommerfeld, Validation of a stochastic Lagrangian modelling approach for inter-particle collisions in homogeneous isotropic turbulence, Int. J. Multiphase Flow **27**, 1829 (2001).
[28] N. Almohammed and M. Breuer, Modeling and simulation of agglomeration in turbulent particle-laden flows: A comparison between energy-based and momentum-based agglomeration models, Powder Technol. **294**, 373 (2016).
[29] T. S. Lundgren, Linearly forced isotropic turbulence, in *Annual Research Briefs 2003* (Center for Turbulence Research, Stanford, CA, 2003), pp. 461–473.
[30] C. Rosales and C. Meneveau, Linear forcing in numerical simulations of isotropic turbulence: Physical space implementations and convergence properties, Phys. Fluids **17**, 095106 (2005).
[31] R. Di Felice, The voidage function for fluid-particle interaction systems, Int. J. Multiphase Flow **20**, 153 (1994).
[32] P. G. T. Saffman, The lift on a small sphere in a slow shear flow, J. Fluid Mech. **22**, 385 (1965).
[33] S. I. Rubinow and J. B. Keller, The transverse force on a spinning sphere moving in a viscous fluid, J. Fluid Mech. **11**, 447 (1961).
[34] S. Chen, W. Liu, and S. Li, A fast adhesive discrete element method for random packings of fine particles, Chem. Eng. Sci. **193**, 336 (2019).
[35] B. Sümer and M. Sitti, Rolling and spinning friction characterization of fine particles using lateral force microscopy based contact pushing, J. Adhes. Sci. Technol. **22**, 481 (2008).
[36] M. Yang, S. Li, and Q. Yao, Mechanistic studies of initial deposition of fine adhesive particles on a fiber using discrete-element methods, Powder Technol. **248**, 44 (2013).
[37] S. Q. Li and J. S. Marshall, Discrete element simulation of micro-particle deposition on a cylindrical fiber in an array, J. Aerosol Sci. **38**, 1031 (2007).

[38] S. Chen, S. Q. Li, and M. Yang, Sticking/rebound criterion for collisions of small adhesive particles: Effects of impact parameter and particle size, Powder Technol. **274**, 431 (2015).
[39] W. Liu, S. Q. Li, A. Baule, and H. A. Makse, Adhesive loose packings of small dry particles, Soft Matter **11**, 6492 (2015).
[40] W. Liu, Y. Jin, S. Chen, H. A. Makse, and S. Q. Li, Equation of state for random sphere packings with arbitrary adhesion and friction, Soft Matter **13**, 421 (2017).
[41] J. S. Marshall, Viscous damping force during head-on collision of two spherical particles, Phys. Fluids **23**, 013305 (2011).
[42] F. L. Yang and M. L. Hunt, Dynamics of particle-particle collisions in a viscous liquid, Phys. Fluids **18**, 121506 (2006).
[43] H. E. Fayed and S. A. Ragab, Direct numerical simulation of particles-bubbles collisions kernel in homogeneous isotropic turbulence, J. Comput. Multiphase Flows **5**, 167 (2013).
[44] X. Jin and J. S. Marshall, The role of fluid turbulence on contact electrification of suspended particles, J. Electrost. **87**, 217 (2017).
[45] H. R. Pruppacher and J. D. Klett, *Microphysics of Clouds and Precipitation* (Springer Netherlands, Heidelberg, 2010).
[46] R. Onishi, K. Takahashi, and S. Komori, Influence of gravity on collisions of monodispersed droplets in homogeneous isotropic turbulence, Phys. Fluids **21**, 125108 (2009).
[47] P. J. Ireland, A. D. Bragg, and L. R. Collins, The effect of Reynolds number on inertial particle dynamics in isotropic turbulence. Part 2. Simulations with gravitational effects, J. Fluid Mech. **796**, 659 (2016).
[48] S. Krijt, C. Güttler, D. Heißelmann, C. Dominik, and A. G. G. M. Tielens, Energy dissipation in head-on collisions of spheres, J. Phys. D **46**, 435303 (2013).
[49] S. Chen, M. K. Yau, and P. Bartello, Turbulence effects of collision efficiency and broadening of droplet size distribution in cumulus clouds, J. Atmos. Sci. **75**, 203 (2018).
[50] F. F. Dizaji and J. S. Marshall, An accelerated stochastic vortex structure method for particle collision and agglomeration in homogeneous turbulence, Phys. Fluids **28**, 113301 (2016).
[51] Q. Jiang and B. E. Logan, Fractal dimensions of aggregates determined from steady-state size distributions, Environ. Sci. Technol. **25**, 2031 (1991).
[52] J. C. Flesch, P. T. Spicer, and S. E. Pratsinis, Laminar and turbulent shear-induced flocculation of fractal aggregates, AIChE J. **45**, 1114 (1999).
[53] M. H. Waldner, J. Sefcik, M. Soos, and M. Morbidelli, Initial growth kinetics and structure of colloidal aggregates in a turbulent coagulator, Powder Technol. **156**, 226 (2005).
[54] C. Selomulya, R. Amal, G. Bushell, and T. D. Waite, Evidence of shear rate dependence on restructuring and breakup of latex aggregates, J. Colloid Interface Sci. **236**, 67 (2001).
[55] D. Liu, W. Zheng, X. Chen, and M. Liu, Simulation of agglomerate breakage and restructuring in shear flows: Coupled effects of shear gradient, surface energy, and initial structure, Powder Technol. **336**, 102 (2018).
[56] S. K. Friedlander and C. S. Wang, The self-preserving particle size distribution for coagulation by Brownian motion, J. Colloid Interface Sci. **22**, 126 (1966).
[57] S. Vemury and S. E. Pratsinis, Self-preserving size distributions of agglomerates, J. Aerosol Sci. **26**, 175 (1995).
[58] M. L. Eggersdorfer and S. E. Pratsinis, Agglomerates and aggregates of nanoparticles made in the gas phase, Adv. Powder Technol. **25**, 71 (2014).
[59] R. Jullien and P. Meakin, Simple models for the restructuring of three-dimensional ballistic aggregates, J. Colloid Interface Sci. **127**, 265 (1989).
[60] M. Elimelech, X. Jia, J. Gregory, and R. Williams, *Particle Deposition and Aggregation: Measurement, Modelling and Simulation* (Elsevier, Amsterdam, 1998).
[61] L. Pan and P. Padoan, Turbulence-induced relative velocity of dust particles. I. Identical particles, Astrophys. J. **776**, 12 (2013).
[62] L. Pan and P. Padoan, Relative velocity of inertial particles in turbulent flows, J. Fluid Mech. **661**, 73 (2010).

[63] O. Ayala, B. Rosa, and L.-P. Wang, Effects of turbulence on the geometric collision rate of sedimenting droplets. Part 2. Theory and parameterization, New J. Phys. **10**, 075016 (2008).
[64] S. L. Rani, R. Dhariwal, and D. L. Koch, A stochastic model for the relative motion of high Stokes number particles in isotropic turbulence, J. Fluid Mech. **756**, 870 (2014).
[65] F. F. Dizaji, J. S. Marshall, and J. R. Grant, Collision and breakup of fractal particle agglomerates in a shear flow, J. Fluid Mech. **862**, 592 (2019).
[66] M. U. Babler, L. Biferale, L. Brandt, U. Feudel, K. Guseva, A. S. Lanotte, C. Marchioli, F. Picano, G. Sardina, A. Soldati, and F. Toschi, Numerical simulations of aggregate breakup in bounded and unbounded turbulent flows, J. Fluid Mech. **766**, 104 (2015).
[67] J. De Bona, A. S. Lanotte, and M. Vanni, Internal stresses and breakup of rigid isostatic aggregates in homogeneous and isotropic turbulence, J. Fluid Mech. **755**, 365 (2014).
[68] P. J. Ireland, A. D. Bragg, and L. R. Collins, The effect of Reynolds number on inertial particle dynamics in isotropic turbulence. Part 1. Simulations without gravitational effects, J. Fluid Mech. **796**, 617 (2016).
[69] P. Liu and C. M. Hrenya, Cluster-Induced Deagglomeration in Dilute Gravity-Driven Gas-Solid Flows of Cohesive Grains, Phys. Rev. Lett. **121**, 238001 (2018).
[70] J. Bec, S. S. Ray, E. W. Saw, and H. Homann, Abrupt growth of large aggregates by correlated coalescences in turbulent flow, Phys. Rev. E **93**, 031102 (2016).
[71] E. W. Saw, G. P. Bewley, E. Bodenschatz, S. S. Ray, and J. Bec, Extreme fluctuations of the relative velocities between droplets in turbulent airflow, Phys. Fluids **26**, 111702 (2014).